ISSN 0915-633X

NIFS--343

JP9507184

NATIONAL INSTITUTE FOR FUSION SCIENCE

Signal Based Mixing Analysis for the Magnetohydrodynamic Mode Reconstruction from Homodyne Microwave Reflectometry

A. Ejiri, S. Sakakibara and K. Kawahata

(Received - Jan. 9, 1995)

NIFS-343 Mar. 1995

NAGOYA, JAPAN

Signal Based Mixing Analysis for the Magnetohydrodynamic Mode Reconstruction from Homodyne Microwave Reflectometry

Akira Ejiri, Satoru Sakakibara[a)] and Kazuo Kawahata

National Institute for Fusion Science
Furo-cho, Chikusa-ku, Nagoya 464-01 Japan
[a)] *Department of Fusion Science, The Graduate University for Advanced Studies, Furo-cho, Chikusa-ku, Nagoya 464-01, Japan.*

Key Words : Microwave Reflectometry, MHD mode, Mixing Analysis, CHS

A new method 'Signal Based Mixing Analysis', to extract the components which are coherent to a certain reference signal from a noisy signal, has been developed. The method is applied to homodyne microwave reflectometry to reconstruct the radial structure of a magnetohydrodynamic (MHD) mode in heliotron/torsatron Compact Helical System (CHS) [K. Matsuoka *et al.* Plasma Phys. Control. Nuclear Fusion Research 1988 **Vol. 2**, IAEA, Vienna 411 (1989)]. In CHS plasmas, MHD fluctuations measured with magnetic probes show bursts, in which the amplitude and frequency quasi-periodically vary. The signal based mixing analysis uses a set of functions which have the same amplitude and the harmonic frequency as those of the magnetic fluctuations. The product (mixing) of the signal of reflectometer and the functions yields

the amplitude and phase of the coherent components. When the plasma density gradually increases, the measuring position moves radially outward. Thus, the radial structure of MHD modes can be obtained by this method. The analysis indicates several peaks and nodes inside the resonance surface of the MHD mode. In addition, the structure does not propagate radially during a burst.

I. Introduction

The study of fluctuations is very important to understand plasmas. Since plasmas have many degrees of freedom and they are turbulent, phenomena in plasmas have large variety. In addition, fluctuations can play important roles in anomalous transport in plasmas. Although many kinds of diagnostics and method of analyses have been developed, further development of those is required to understand fluctuations. Radial structure of magnetohydrodynamic (MHD) modes is one of the interesting topics in high temperature plasmas, and the structure is a key issue to investigate the validity of MHD theories and to estimate the effect of MHD modes on transport. In short pulse discharges, it is possible to measure the structure of magnetic fluctuations by insertable probes. Excellent work has been done by D. Brotherton-Ratcliffe *et al.*, using the correlation matrix method [1]. By the method, global and local fluctuations are resolved, so that radial structure of global MHD modes was shown. In heliotron/torsatron Compact Helical System (CHS) [2], it is difficult to insert probes due to its long discharge duration and its high temperature. On the other hand, microwave reflectometers can measure deep inside the plasma. The reflectometeric measurement is radially localized. However, special techniques must be developed to investigate global modes, because the reflectometer appears

to be rather insensitive to global modes.

The magnetic fluctuations in CHS are measured by poloidal and toroidal probe array sets just inside the vacuum vessel. Quasi-periodic bursts of the $m/n = 2/1$ mode, where m and n are poloidal and toroidal mode numbers, are observed in low beta plasmas when a neutral beam is injected in co-direction. The magnetic fluctuations are believed to be MHD modes, which causes displacement of magnetic surfaces. Furthermore, MHD modes probably induce density perturbations, because the pressure is a function of magnetic surfaces. In the present analysis, the standard Fourier analysis is not appropriate to investigate the phase and correlation between the magnetic fluctuations and other signals, because the frequency of the magnetic fluctuations quasi-periodically change.

Microwave reflectometry [3] is based on the fact that microwaves in plasmas are reflected at the cutoff layer, where the frequency of the launched microwave coincides with the cutoff frequency of the plasma. The cutoff frequency for O-mode waves is proportional to the square root of density. According to a simple picture, density fluctuations cause movement of the cutoff layer, which behaves as an oscillating mirror causing phase variation in the reflected wave. Therefore, the components coherent to MHD fluctuations give information about the fluctuations induced by the MHD modes at the cutoff layer. During a discharge, the density gradually increases, and the cutoff layer moves radially outward. If the coherent components are extracted, radial structures of MHD modes can be obtained.

Both the magnetic probes and the microwave reflectometer have quite different sensitivities to perturbations. The magnetic probes are located well outside the plasma. They are sensitive to global modes, and cannot reveal radial structure. On the other hand, microwave reflectometer is rather insensitive to global modes, but

sensitive to short wavelength modes at the cutoff layer. Standard correlation analysis cannot reveal correlation between them. Fourier analysis is also ineffective because of the quasi-periodic change in the frequency of the magnetic fluctuations (bursts). In the present paper, the method 'Signal Based Mixing Analysis' is described. By this method, the component that has a certain phase relation to the magnetic bursts can be extracted from the reflectometer signal, even though the component is very small.

This paper is organized in the following manner. In Sec. II., characteristics of MHD signals measured by probes and those of the signal measured by a microwave reflectometer are described. The results from the standard analyses are also presented. Sec. III. describes the principle of the signal based mixing analysis. In Sec. IV., an MHD mode structure is reconstructed by the analysis, and noise level is also estimated. Finally, Sec. V. is reserved for conclusions.

II. Characteristics of MHD and Reflectometer Signals

Magnetic fluctuations show quasi-periodic bursts in low beta plasmas ($\langle\beta\rangle < 0.5\%$) when a neutral beam is injected in co-direction. The fluctuations are coherent in both time and space domains. They have the mode structure of $m/n = 2/1$, and the dominant power is in the range $10 - 100$ kHz (Fig. 1(a)). The oscillation is induced by the rotation of the mode in the ion diamagnetic direction. Figure 2(a) shows the time evolution of the magnetic fluctuations in the frequency range of $10 - 100$ kHz. During a single burst, the frequency calculated from zero-crossing times shows the sawtooth modulation (Fig. 2(b)). The broad power spectrum (Fig. 1(a)) is due to the frequency modulation, rather than due to turbulent behavior.

A microwave reflectometer has been installed in the CHS device to measure

electron density fluctuations. It views a central chord of the horizontally elongated plasma. A circular horn antenna and a circular window made of fused quartz are used. It has three Gunn oscillators with the frequencies of 27, 33, 39 GHz. The launched microwave frequency can be changed by a rotary switch shot by shot. The system is operated in homodyne mode. In contrast to the magnetic fluctuations, the reflectometer signal is turbulent (Fig. 2(c)), and the power spectrum is very broad (Fig. 1(b)).

The Fourier analysis is useful when a certain (fixed) frequency component is dominant, but in the present case, it is not useful as shown in the following. Figures 3(a), (b) show the coherence and phase between magnetic fluctuations which are measured at two poloidally separated (82°) positions. The magnetic fluctuations have high coherence along both poloidal and toroidal directions, and phase is well defined. On the other hand, the coherence between the reflectometer signal and the magnetic fluctuations is as low as the level of incoherent signals (Fig. 3(c)). The expected value of the coherence between two random signals is $1/N$, where N is the number of the ensemble [4]. In the present analysis, N is 20, and the coherence between reflectometer signal and magnetic fluctuations is almost the same level as those between random signals. Therefore, the Fourier analysis shows no coherence between both signals.

The cross-correlation is an appropriate representation of the relation between two signals when one wave propagates with a constant velocity. In the present case, however, it is not appropriate as shown in the following. Figure 4(a) shows the normalized cross-correlation (cross-correlation function) between magnetic fluctuations at two positions. The function exhibits peaks, amplitude of which is close to unity around zero time lag. The peaks around $\tau = \pm 0.6$ msec represent the

correlation between succeeding two bursts. The cross-correlation function between the magnetic fluctuations and the reflectometer signal exhibits much smaller peaks. A small peak with the height of 0.1 around $\tau = 0$ msec can be seen. This peak probably represents the coherent components, but the height is almost the same as those of the peaks at $\tau \neq 0$, which is probably noise. From these analyses, either the correlation between the magnetic fluctuations and the reflectometer signal is small or they are incoherent.

III. Signal Based Mixing Analysis

The basic idea for the extraction of components having a certain phase relation to the reference signal is to use functions similar to the reference, while Fourier analysis uses sinusoidal waves. This analysis is similar to the mixing process in communication systems, in which low frequency messages are extracted from high frequency transmission signals. Let f_1 be the frequency of a transmitted signal, which includes carrier frequency f_0 and the low frequency information. The local frequency of a receiver is adjusted to be f_0. The process of mixing of two signals with frequencies of f_0 and f_1, yields signals with the lower frequency of $|f_0 - f_1|$ and higher frequency of $f_0 + f_1$. Applying a low pass filter we can exclude the higher frequency component. Thus, the mixing process is quite useful in extracting the low frequency information even though the carrier frequency fluctuates. Let $y_{FM}(t)$ be the local (reference) signal,

$$y_{FM}(t) \propto \sin\left(2\pi \tilde{f}_0 t\right) , \tag{1}$$

where $\tilde{f}_0$ is a fluctuating frequency. This is an FM signal. The time scale of the frequency modulation is much longer than the period of the oscillation $1/\tilde{f}_0$. Suppose

that the phase of the reflectometer signal (reflected wave) has the same frequency as the local signal:

$$\Phi(t) = \Phi_0 \sin(2\pi \tilde{f}_0 t + \phi_0) \ . \tag{2}$$

Nonlinear response of a homodyne microwave reflectometer must be taken into account. A homodyne microwave reflectometer measures $\sin\Phi(t)$, where $\Phi(t)$ is phase of reflected wave. The component coherent to the reference (local) signal (Eq.(2)) can be written as $\sin(\Phi_0 \sin(2\pi \tilde{f}_0 t + \phi_0))$. We assume that the signal of reflectometer y_1 consists of the coherent and incoherent components, and the incoherent component has no correlation to the local signal. The signal y_1 is then written as

$$y_1(t) = \tilde{y}_{incoh}(t) + \sin(\Phi_0 \sin(2\pi \tilde{f}_0 t + \phi_0)) \ . \tag{3}$$

In general, double sin function can be expanded by harmonic waves, the coefficients of which are represented by Bessel functions [5]. Thus, Eq. (3) can be written as

$$\begin{aligned} y_1(t) &= \tilde{y}_{incoh}(t) + a_1 \sin(2\pi \tilde{f}_0 t + \phi_1) + a_2 \sin(2\pi 2\tilde{f}_0 t + \phi_2) + \ldots \\ &\quad + a_j \sin(2\pi j \tilde{f}_0 t + \phi_j) + \ldots \qquad (j = 1, 2, \ldots) \\ &= \tilde{y}_{incoh}(t) + \sum_{j=1}^{\infty} a_j \sin(2\pi j \tilde{f}_0 t + \phi_j) \end{aligned} \tag{4}$$

In order to extract coherent components, harmonic mixing is used. The local function is

$$y_{FM}(t; \Delta\phi, n) \equiv \sin(2\pi n \tilde{f}_0 t + \Delta\phi) \qquad (n = 1, 2, \ldots) \ , \tag{5}$$

where $\Delta\phi$ is a parameter. When we mix $y_1(t)$ with fundamental signal $y_{FM}(t; \Delta\phi, n = 1)$, the coefficient of the fundamental coherent component can be derived. The output of mixing is written as

$$y_1(t) \otimes y_{FM}(t; \Delta\phi, n = 1)$$

$$
\begin{aligned}
&= \left(\tilde{y}_{incoh}(t) + \sum_{j=1}^{\infty} a_j \sin(2\pi j \tilde{f}_0 t + \phi_j)\right) \times \sin(2\pi \tilde{f}_0 t + \Delta\phi) \\
&= \tilde{y}_{incoh}(t)\sin(2\pi \tilde{f}_0 t + \Delta\phi) + a_1 \sin(2\pi \tilde{f}_0 t + \phi_1)\sin(2\pi \tilde{f}_0 t + \Delta\phi) \\
&\quad + a_2 \sin(2\pi 2\tilde{f}_0 t + \phi_2)\sin(2\pi \tilde{f}_0 t + \Delta\phi) + \ldots \\
&= \tilde{y}_{incoh}(t)\sin(2\pi \tilde{f}_0 t + \Delta\phi) \\
&\quad + \frac{1}{2}\sum_{j=1}^{\infty} a_j \left(\cos(2\pi(j-1)\tilde{f}_0 t + \phi_j - \Delta\phi) - \cos(2\pi(j+1)\tilde{f}_0 t + \phi_j + \Delta\phi)\right) \quad (6)
\end{aligned}
$$

Applying a low pass filter, the fundamental component can be extracted. The cutoff frequency is chosen to be lower than oscillating frequency $\tilde{f}_0$. Then, the right hand side of Eq. (6) is written as

$$
\left[\tilde{y}_{incoh}(t)\sin(2\pi \tilde{f}_0 t + \Delta\phi)\right]_{f<f_{cut}} + \frac{1}{2} a_1 \cos(\phi_j - \Delta\phi) \; . \quad (7)
$$

Since the first term is incoherent to the local signal by the definition, it can be eliminated. In the same manner, when we mix $y_1(t)$ with the harmonic signal $y_{FM}(t; \Delta\phi, n)$, the coefficient of nth coherent component can be derived. The extracted component includes phase $(\phi_n - \Delta\phi)$ and amplitude (a_n) information. Changing the parameter $\Delta\phi$, the amplitude and the relative phase can be resolved as described in Sec. IV..

In the above, an FM local signal is used. When the reference signal shows amplitude modulation in addition to frequency modulation, this feature is useful for the improvement of sensitivity to coherent components. As show in Fig. 2(a), during a burst, the amplitude of magnetic fluctuations changes. Using this feature, the sensitivity to the components which have similar amplitude variation (burst) can be improved. For this purpose, the local signal takes the form $Y(t)\sin(2\pi n \tilde{f}_0 t + \Delta\phi)$, where $Y(t)$ is a positive amplitude varying much slower than the oscillation $\tilde{f}_0$. The

FM/AM modulated local function set is

$$y_{FM/AM}(t;\Delta\phi,n) \equiv Y(t)_{norm}\sin(2\pi n\tilde{f}_0 t + \Delta\phi) \qquad (n = 1,2,\ldots)\ , \tag{8}$$

where $Y(t)_{norm}$ is the normalized amplitude defined as

$$Y(t)_{norm} \equiv \frac{Y(t)}{1/\tau\int_{t-\tau/2}^{t+\tau/2} Y(s)ds}\ , \tag{9}$$

where τ is the time scale much longer than the bursts. This method puts higher weight on the time when the amplitude of the local signal is large. The amount of improvement in sensitivity depends on the degree of modulation. The sensitivity can be defined as the ratio of the amplitude of coherent components to the rms amplitude of an objective signal. In the case of sinusoidal amplitude modulation for both local and objective signals, 100% amplitude modulation case improves the sensitivity by 50%, and 50% modulation case yields 13% improvements.

IV. Application

Firstly, radial structure of an MHD mode is presented by calculating the fundamental component ($n = 1$). Secondly, a method of estimating noise level is described, and applied for the reconstructed MHD mode. Thirdly, higher harmonic components ($n \neq 1$) are calculated to estimate the phase fluctuation amplitude of the reflected wave.

A. Reconstruction of an MHD mode

The signal based mixing analysis has been applied to the signal of microwave reflectometry to extract the component coherent to the magnetic fluctuations. Figure 5(a) illustrates the block diagram of the analysis. The objective signal y_1 and

the reference signal y_0 are input signals, and the phase delay $\Delta\phi$ and the harmonic number n are given parameters of the analysis. In the present analysis, y_0 and y_1 are chosen to be the magnetic fluctuation and the reflectometer signal, respectively. The analysis has two types of outputs, which are coherent components. One uses an FM signal and the other uses a normalized FM/AM signal as local signals. The FM local signal y_{FM} is created from zero-crossing times t_j $(j = 1, 2, \ldots)$ of the reference signal. Sinusoidal waves are used for each time period as

$$y_{FM}(t; \Delta\phi, n) \equiv \pm \sin\left(\pi n \frac{t - t_j}{t_{j+1} - t_j} + \Delta\phi\right) \qquad (t_j < t < t_{j+1}) \,, \tag{10}$$

where the sign is set to be the same as y_0. The FM signal has constant amplitude of unity (Fig. 6(b)). Note that it is easy to apply phase shift to the function (Eq. (10)). The rms of y_0 yields the amplitude $Y(t)$. The time window for the calculation of rms is set to be larger than the oscillation period. The product of $Y(t)$ and y_{FM} gives the FM/AM local signal. In order to normalize the amplitude, the smoothed (with the time window of 5.12 msec) amplitude is calculated by the moving average method. The time window is chosen to be much longer than the period of bursts. Then, the FM/AM reference is divided by the time smoothed amplitude to obtain the normalized FM/AM local signal $y_{FM/AM}$ (Fig. 6(c)). After the mixing between the reflectometer signal and the local signals, a low pass filter with the cutoff frequency of 0.5 kHz is used to get coherent components. Hereafter, we call this output of the mixing analysis FM mixing output or FM/AM mixing output. Changing the phase delay parameter, we can obtain the phase relation between the coherent component and magnetic fluctuations and its amplitude. Quadrature phase calculation is used to separate the mixing output into the amplitude and phase (Fig. 5(b)). This method uses two mixing outputs with the phase delay parameter of $\Delta\phi = 0, 90°$.

In a discharge, the density gradually increases (Fig. 7(a)). The density profile

is measured with an HCN laser interferometer [6] using five identical discharges. The density profile is well represented by parabolic profiles. The present analysis has been done for the other shot with slightly different level of plasma current. Therefore, parabolic density profiles are assumed, and the central chord averaged electron density is used to reconstruct density profiles. Using these profiles, the position of the cutoff layer is calculated. The cutoff layer appears at $t = 47$ msec, and the layer moves outward gradually (Fig. 7(b)). Figures 7(c),(d) shows the FM and FM/AM mixing outputs. They exhibit several peaks around $t = 70$ msec, when the normalized radius of the cutoff layer is around 0.5.

The amplitude of the reflectometer signal tends to increase as the cutoff layer moves outward. This is because the distance between the antenna and the cutoff layer changes, and the curvature of the layer changes. To correct the change in reflected power, the FM/AM mixing output is normalized by the rms amplitude of the reflectometer signal. The normalized FM/AM mixing output is around 0.1, while the completely coherent signals yield the output of 0.5 (see Sec. IV.-B.). Thus, the coherent component is much smaller than incoherent components. This fact is consistent with the results of Fourier and cross-correlation analyses (Figs. 3(c), 4(b)), which show small or no correlation.

When the reference signal has amplitude modulation, FM/AM mixing can give higher sensitivity to coherent components than FM mixing as described in Sec. III.. In the present case, however, the amplitude modulation is about 40%, and the sensitivity can be improved only by about 10%. Thus, the FM and FM/AM mixing outputs show almost the same behavior, and the improvement is not significant (Figs. 7(c),(d)).

Figure 8 shows the FM/AM mixing outputs of the reflectometer signal as a

function of the normalized minor radius for several values of $\Delta\phi$. The data from $t = 50$ msec to 120 msec is shown. Before $t = 50$ msec, the cutoff layer rapidly moves, and the mixing output is reduced due to the low pass filter of the final stage of the mixing analysis. The data after $t = 120$ msec is not shown because the mode structure of the magnetic fluctuations begins to change from this time. The outputs exhibit several clear peaks at $\rho < 0.6$, where ρ is the normalized minor radius. As shown in Sec. IV.-B., these are well above the noise level. On the other hand, structures at $\rho > 0.6$ are small and they have the same level as the noise. The radius of the rational surface ($\iota/2\pi = 0.5$), which is the resonance surface of $m/n = 2/1$ mode, is calculated from the 3-D MHD equilibrium code VMEC [7]. Since the plasma current changes during the discharge, the radius varies between the dashed lines in Fig. 8. The coherent components have several peaks inside the rational surface. The wavelength of the mode is in the range $0.05a \sim 0.1a$ at $0.5 < \rho < 0.6$. A structure with a longer wavelength is seen inside the $\rho = 0.5$ radius. These components ($\rho < 0.6$) do not radially propagate, and there are several nodes where amplitude is zero. Dotted lines in Fig. 8 indicate some of these nodes. The mode is believed to be pressure driven interchange modes [8], and the features derived by the present method are consistent with the expectation from MHD theory.

B. Estimation of noise level

The performance of the signal based mixing analysis can be measured by sensitivities to coherent and incoherent components. An ideal method has high sensitivity to coherent components and low (or zero) sensitivity to incoherent components. If the analysis has finite sensitivity to incoherent component, the sensitivity determines the noise level of the analysis. In other words, noise of the present analysis

arises from residual incoherent components. One of the means to estimate the ratio of these sensitivities, is to compare the mixing outputs of completely coherent and completely incoherent signals.

When we chose the same signal for both the reference and objective signals, the objective signal is completely coherent to the reference signal. Obtaining completely incoherent signals is relatively difficult. Since coherent components are defined as the components having a certain phase relation to the reference signal, completely incoherent components have random phase relation to the reference signal. In addition, to make an accurate comparison between coherent and incoherent signals, the other features such as power spectrum should be the same. One of the easy methods to make an almost incoherent signal is using a time delayed signal. As shown in Fig. 4(a), the correlation can be very small at finite time lag. Furthermore, the power spectra are almost same for the original and the delayed signals as far as the amount of time delay is small. Using this method, the upper bound for the noise level can be determined.

Magnetic fluctuation is used for the reference and objective signals. We chose delay times τ_{delay} as $0, 0.3, 0.8, 1.0$ msec. The signal with $\tau_{delay} = 0$ msec is the completely coherent signal. The other delayed signals are almost incoherent signals. Three signals with different τ_{delay} is analyzed to examine the statistical scatter of the noise level. Note that the delay time $\tau_{delay} \sim \pm 0.6$ msec is avoided, because the correlation at that time lag is high (Fig. 4(a)). Instead of mixing outputs, positive definite amplitudes, which are obtained by the quadrature phase calculation (Fig. 5(b)), are used to make the comparison. Figure 9 shows the amplitudes as a function of ρ. The amplitude for the completely coherent signal is 0.5. This value corresponds to the coefficient $1/2$ in the second term of Eq. (7). In this case, the value of a_1 in

the equation is unity because of the normalization process in the FM/AM mixing analysis. On the other hand, the almost incoherent signals yield much smaller amplitudes. The amplitude is not constant but varies with ρ. This variation is mainly due to the statistical scatter of noise (residual incoherent components), because the amplitudes with different delay times show different behavior. The averaged noise show smaller variation (Fig. 9(a)), and it is almost constant as ρ increases. As a result, the ratio of sensitivities to coherent and incoherent components is more than about 10.

Now we estimate the noise (residual incoherent components) for the reconstructed MHD mode. The noise is calculated in the same manner, using delay times of $\tau_{delay} = 0.3, 0.8, 1.0$ msec. The amplitude of FM/AM mixing output includes amplitudes of coherent and residual incoherent components. Figure 10 shows the amplitudes as a function of ρ. Assuming that the noise is constant and the variation is due to statistical error, $\pm 1\sigma$ range of the noise level is drawn. The structure at $\rho < 0.6$ is well above the noise level. However, that at $\rho > 0.6$ is the same as the noise level, and we cannot observe mode structure at this region.

C. Harmonic components

In the above two sections, the results of fundamental components are presented. Here, the higher harmonic components ($n \neq 1$) are calculated. The harmonic components can arise from the coherent components which deviate from the fundamental sinusoidal component. Two cases are possible. One is that the reference signal itself has deviation from the fundamental sinusoidal component which is used for the fundamental local signal. However, the magnetic fluctuations are well represented by fundamental sinusoidal waves (Fig. 6(a)), and the higher harmonic components are

more than an order of magnitude smaller than the fundamental component. The other case is that the objective signal is a nonlinear function of the reference signal. The latter case occurs for homodyne microwave reflectometry, which responses nonlinearly to the phase of reflected waves. Because the effect of nonlinear response becomes significant when the amplitude of phase fluctuation (Eq. (2)) exceeds 2π, a comparison of the amplitude of harmonic components yields information about the magnitude of phase fluctuation.

The magnitude can be estimated as the following, although homodyne systems cannot distinguish phase variation and amplitude variation. When the phase variation becomes larger than about 2π, the amplitude is limited and the signal shows folding, which results in higher harmonic frequency components [9]. Thus, we can estimate the magnitude of phase variation by comparing the amplitudes of harmonic components. Figure 11 shows the amplitude of FM/AM mixing outputs for harmonic numbers of $n = 1$, 2, 3 and 4. Dotted lines show the range of the noise level calculated by the same method previously described. The amplitudes with the harmonic number of $n = 2$, 3 and 4 are almost same as the noise levels, and the possible amplitudes of coherent components are smaller than the fundamental one at $\rho < 0.6$. Thus, we can conclude that the amplitude of phase fluctuation at $\rho < 0.6$ is less than about 2π. Due to the low S/N ratio, more accurate estimation is impossible.

V. Conclusions

A new method 'Signal Based Mixing Analysis', to extract the components which are coherent to a certain reference signal from a noisy signal, has been developed. The method is applied to homodyne microwave reflectometry to extract the compo-

nents coherent to $m/n = 2/1$ MHD fluctuations, and radial structure of the MHD mode is reconstructed. The radial structure has several peaks and nodes inside the resonance surface ($\rho \sim 0.6$). The wavelength at $0.5 < \rho < 0.6$ is in the range $0.05a \sim 0.1a$. In addition, the structure does not radially propagate. No structure has been observed outside the resonance surface. A comparison of higher harmonic amplitudes indicates that the phase variation of the reflected wave is less than about 2π.

While Fourier analysis uses sinusoidal waves as a set of functions, the signal based mixing analysis uses functions which have the same amplitude and the harmonic frequency as those of a reference signal. In other words, the method expands an objective signal by a set of functions which are similar to the reference signal. In this sense, the method is an extension of the wavelet analysis. The application to the homodyne microwave reflectometer is successful, however, the obtained results are rather qualitative. This is mainly due to the nonlinear response of the homodyne reflectometer. In addition, the principle of microwave reflectometry is not fully understood, and physical interpretation of the results must be carefully done.

Acknowledgements

The authors wish to thank M. Kando for useful discussion. They would like to thank K. Tanaka for density profile measurements. They are also grateful to the CHS staff for the supports during the experiments.

REFERENCE

[1] D. Brotherton-Ratcliffe, C.G. Gimblett and I.H. Hutchinson, Plasma Phys. Control. Fusion, **29**, 161 (1987).

[2] K. Matsuoka, S. Kubo, M. Hosokawa, Y. Takita, S. Okamura, N. Noda, H. Yamada, H. Iguchi, K. Masai, S. Morita, K. Ida, H. Idei, C. Takahashi, K. Nishimura, T. Shoji, H. Sanuki, M. Fujiwara, Y. Abe, T. Amano, A. Ando, T. Aoki, D.-G. Bi, J. Fujita, S. Hidekuma, T. Kamimura, O. Kaneko, T. Kawamoto, A. Mohri, A. Nishizawa, S. Tanahashi, J. Todoroki, K. Tsuzuki and K. Yamazaki in Plasma Phys. Control. Nuclear Fusion Research 1988 proc. 12th IAEA Int. Conf., Nice,1988 **Vol. 2**, IAEA, Vienna 411 (1989).

[3] C.A.J. Hugenholtz, RR 90-192, FOM-Instituut voor Plasmafysica Rijnhuizen, Nieuwegein (1990).

[4] A. Ejiri (private communication, 1992)

[5] e.g. S. Moriguchi, K. Udagawa and S. Ichimatsu, Mathematical Formula III, (Iwanami, Tokyo, 1960), p.211 (in Japanese).

[6] K. Tanaka, K. Toi, A. Ejiri, K. Kawahata, S. Kubo, H. Arimoto, S. Okajima, S. Okamura, H. Iguchi, S. Sakakibara, T. Morisaki, K. Ida, H. Yamada, S. Morita, K. Tsumori, R. Akiyama, H. Idei, O. Kaneko, A. Komori, K. Matsuoka, K. Nishimura, A. Sagara, C. Takahashi, Y. Takita, J. Xu and I. Yamada, in *Proc. of the 21st European Conf. on Controlled Fusion and Plasma Physics*, **18B Pt. 1** 432 (1994).

[7] S.P. Hirshman and W.I. van Rij, Comput. Phys. Commun., **43** 143 (1986).

[8] S. Sakakibara, H. Yamada, A. Ejiri, K. Ida, K. Matsuoka, T. Morisaki, S. Morita, O. Motojima, K. Nishimura, S. Okamura, C. Takahashi, K. Toi and K. Watanabe, J. Phys. Soc. Jpn., **63** (1994).

[9] G.J. Kramer, A.C. Sips and N.J. Lopes Cardozo, Plasma Phys. Control. Fusion, **35**, 1685 (1993).

Figure 1. Power spectral density of magnetic fluctuations b (a), and that of the reflectometer signal (b).

Figure 2. Time evolution of magnetic fluctuations (a), zero-crossing frequency (b) and reflectometer signal (c).

Figure 3. Coherence (a) and phase difference (b) between magnetic fluctuations measured at two poloidal positions. And the coherence (c) between magnetic fluctuations and reflectometer signal.

Figure 4. Cross-correlation function between magnetic fluctuations measured at two poloidal positions (a), and that between magnetic fluctuations and reflectometer signal (b) as a function of lag.

Figure 5. Block diagram of the signal based mixing analysis (a), and that of quadrature phase calculation (b).

Figure 6. The signal of a magnetic probe (a), and the FM (b) and normalized FM/AM (c) local signals created from the probe signal.

Figure 7. Temporal behaviors of the line averaged density (a), normalized radius of the cutoff layer (b), FM mixing output (c), and FM/AM mixing output (d).

Figure 8. FM/AM mixing output as a function of normalized radius ρ for various phase delay. Solid lines are guide to show zero levels, and dashed lines show the range where the rational surface ($\iota/2\pi = 0.5$) exists, and dotted lines indicate the position of three nodes.

Figure 9. Amplitudes of FM/AM mixing output for $\tau_{delay} = 0$ (a), 0.3 (b), 0.8 (c), 1.0 msec (d) as a function of ρ. The average amplitude of $\tau_{delay} = 0.3, 0.8, 1.0$ msec is also shown in Fig. (a).

Figure 10. Amplitudes of FM/AM mixing output (thick solid curve), which includes coherent and residual incoherent (noise) components, and residual

incoherent (noise) components (dotted curve). $\pm 1\sigma$ range of the noise level (thin solid lines) is also drawn.

Figure 11. Amplitude of FM/AM mixing output for harmonic numbers of n =1, 2, 3 and 4. Dotted lines show the $\pm 1\sigma$ range of the noise level, and dashed lines show the range of the rational surface.

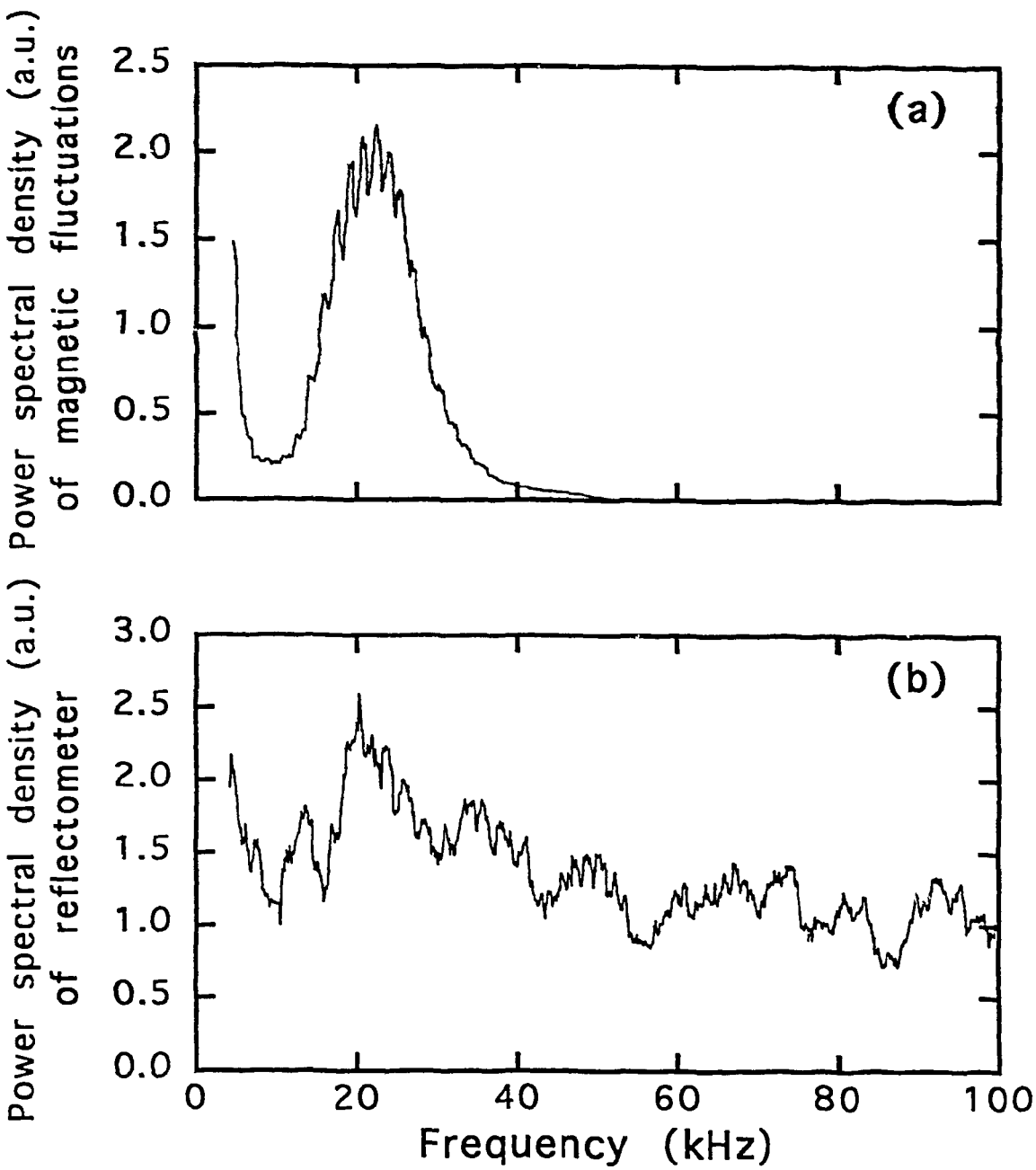
Power spectral density (a.u.) of magnetic fluctuations
2.5
2.0
1.5
1.0
0.5
0.0
(a)
Power spectral density (a.u.) of reflectometer
3.0
2.5
2.0
1.5
1.0
0.5
0.0
(b)
0
20
40
60
80
100
Frequency (kHz)

Fig.1

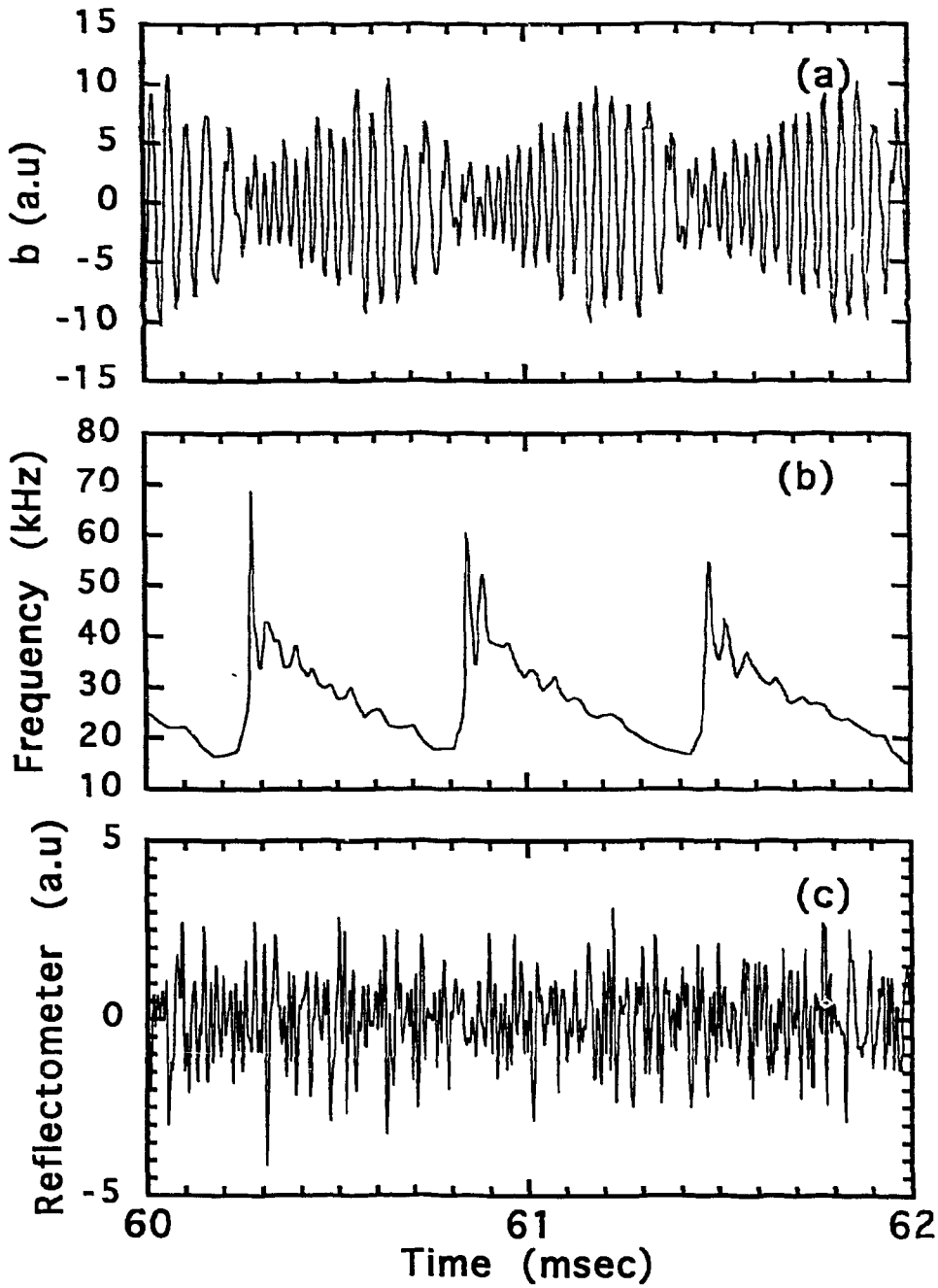
15
10
5
0
-5
-10
-15
b (a.u)
(a)
80
70
60
50
40
30
20
10
Frequency (kHz)
(b)
5
0
-5
Reflectometer (a.u)
(c)
60
61
62
Time (msec)

Fig.2

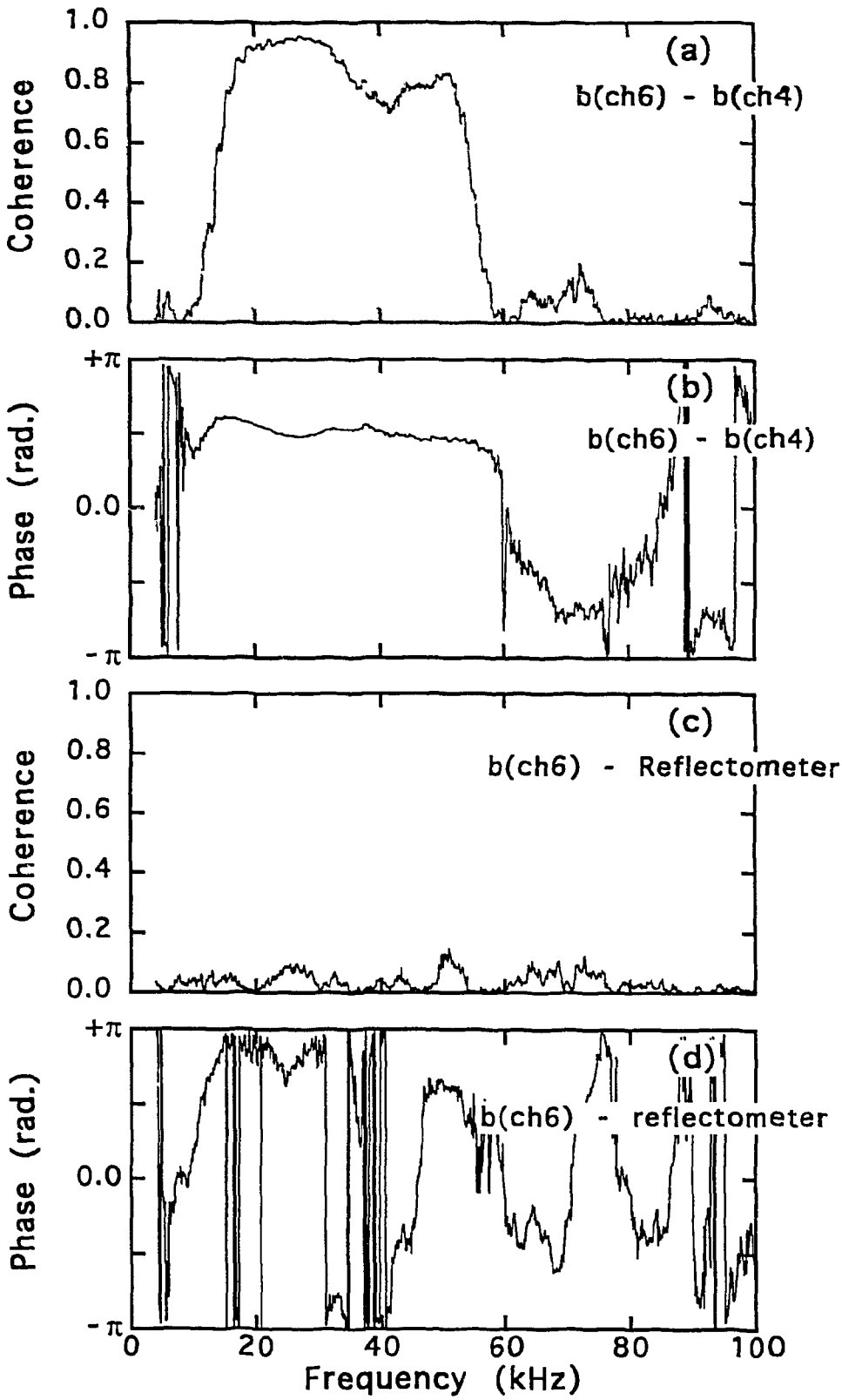
1.0
0.8
0.6
0.4
0.2
0.0
Coherence
(a)
b(ch6) - b(ch4)
+π
0.0
-π
Phase (rad.)
(b)
b(ch6) - b(ch4)
1.0
0.8
0.6
0.4
0.2
0.0
Coherence
(c)
b(ch6) - Reflectometer
+π
0.0
-π
Phase (rad.)
(d)
b(ch6) - reflectometer
0
20
40
60
80
100
Frequency (kHz)

Fig.3

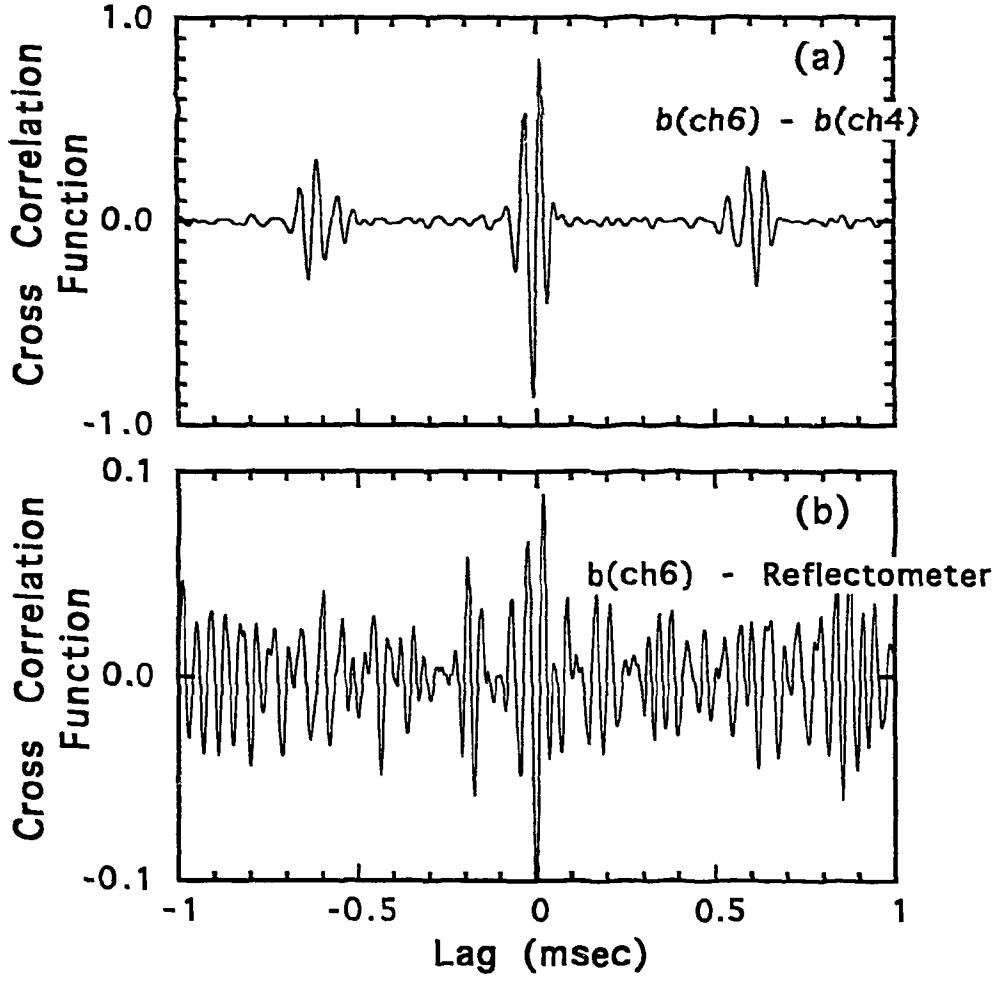
1.0
0.0
-1.0
Cross Correlation Function
(a)
b(ch6) - b(ch4)
0.1
0.0
-0.1
Cross Correlation Function
(b)
b(ch6) - Reflectometer
-1
-0.5
0
0.5
1
Lag (msec)

Fig.4

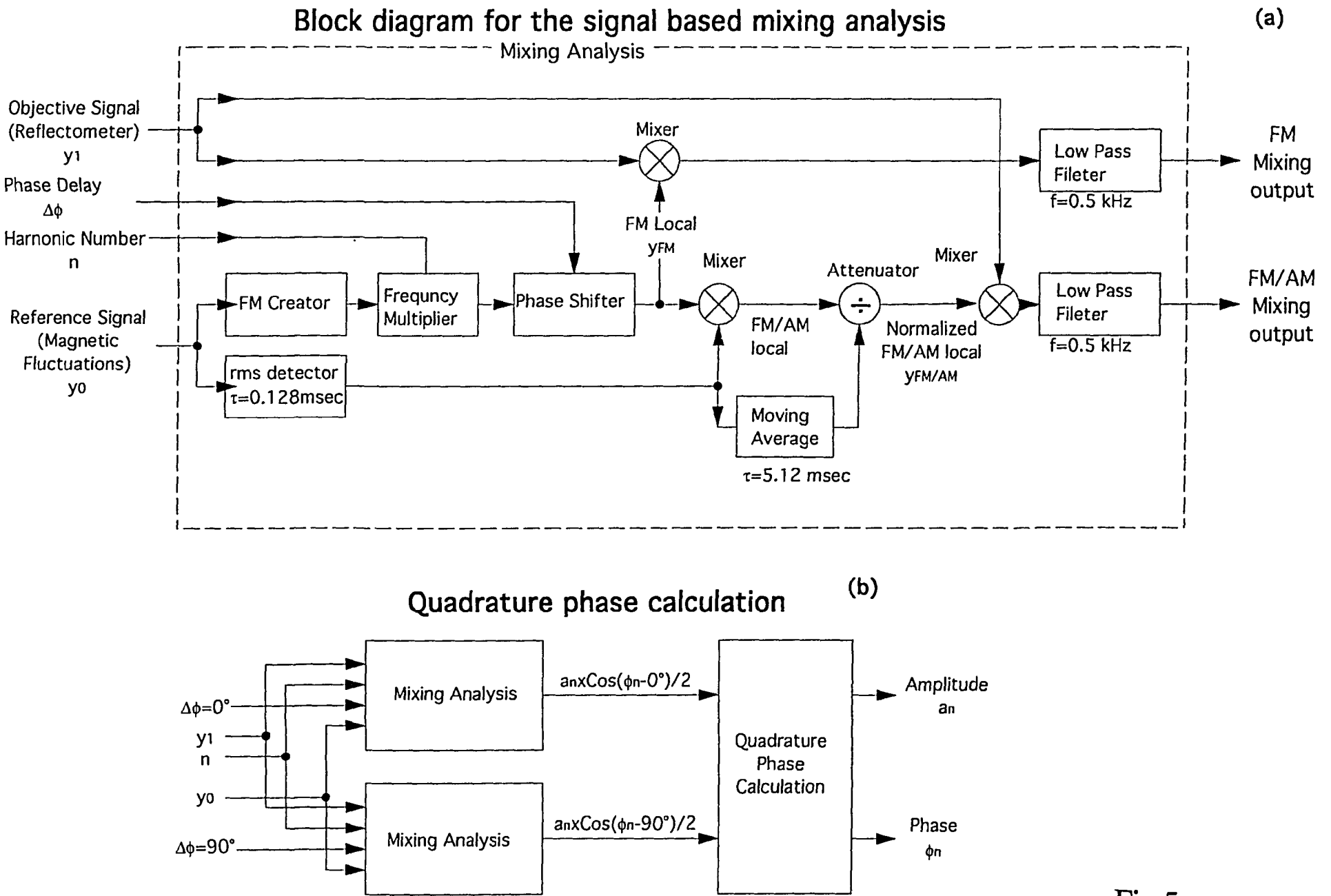
Block diagram for the signal based mixing analysis
(a)
Mixing Analysis
Objective Signal
(Reflectometer)
y1
Phase Delay
Δϕ
Harnonic Number
n
Reference Signal
(Magnetic
Fluctuations)
y0
FM Creator
Frequncy
Multiplier
Phase Shifter
Mixer
FM Local
yFM
Mixer
FM/AM
local
Attenuator
Normalized
FM/AM local
yFM/AM
Mixer
Low Pass
Fileter
f=0.5 kHz
FM
Mixing
output
Low Pass
Fileter
f=0.5 kHz
FM/AM
Mixing
output
rms detector
τ=0.128msec
Moving
Average
τ=5.12 msec
Quadrature phase calculation
(b)
Δϕ=0°
y1
n
y0
Δϕ=90°
Mixing Analysis
Mixing Analysis
anxCos(ϕn-0°)/2
anxCos(ϕn-90°)/2
Quadrature
Phase
Calculation
Amplitude
an
Phase
ϕn

Fig.5

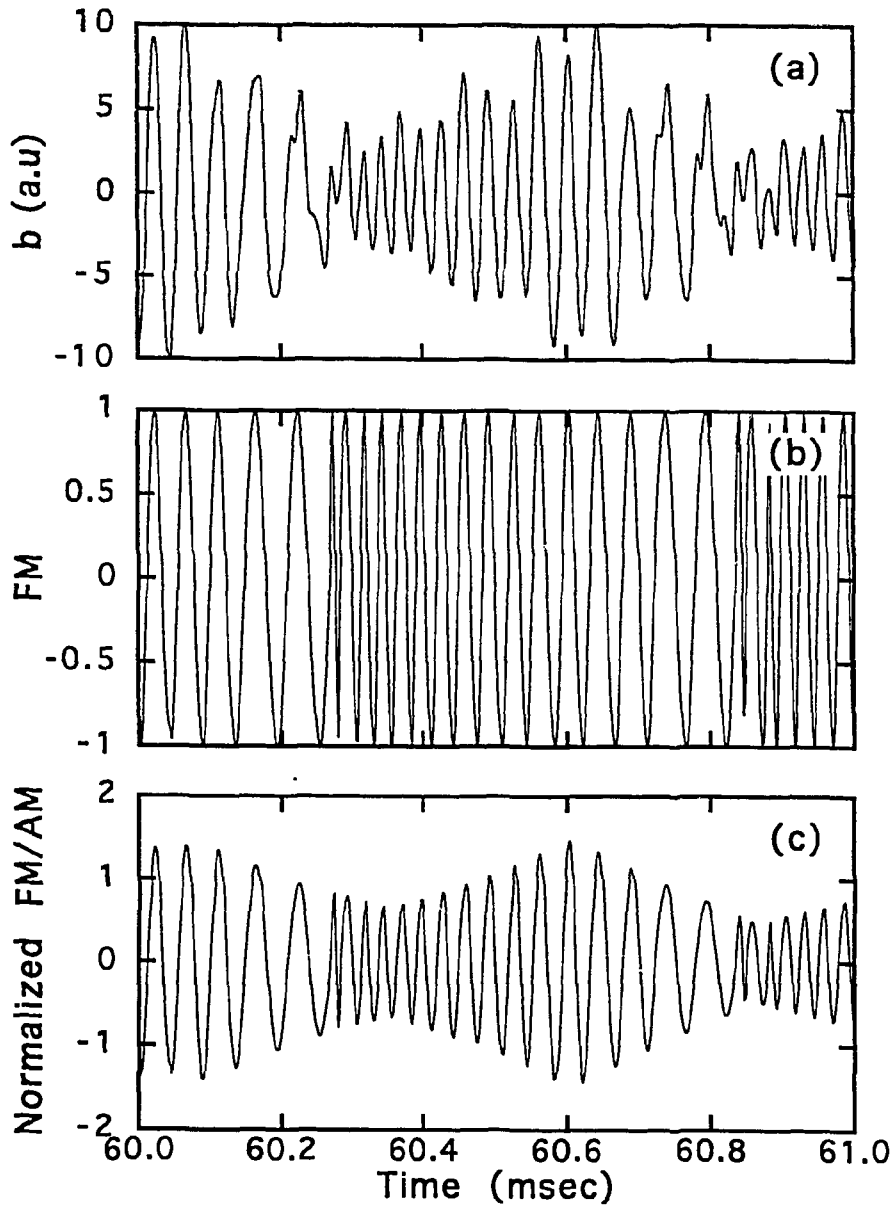
10
5
0
-5
-10
b (a.u)
(a)
1
0.5
0
-0.5
-1
FM
(b)
2
1
0
-1
-2
Normalized FM/AM
(c)
60.0
60.2
60.4
60.6
60.8
61.0
Time (msec)

Fig.6

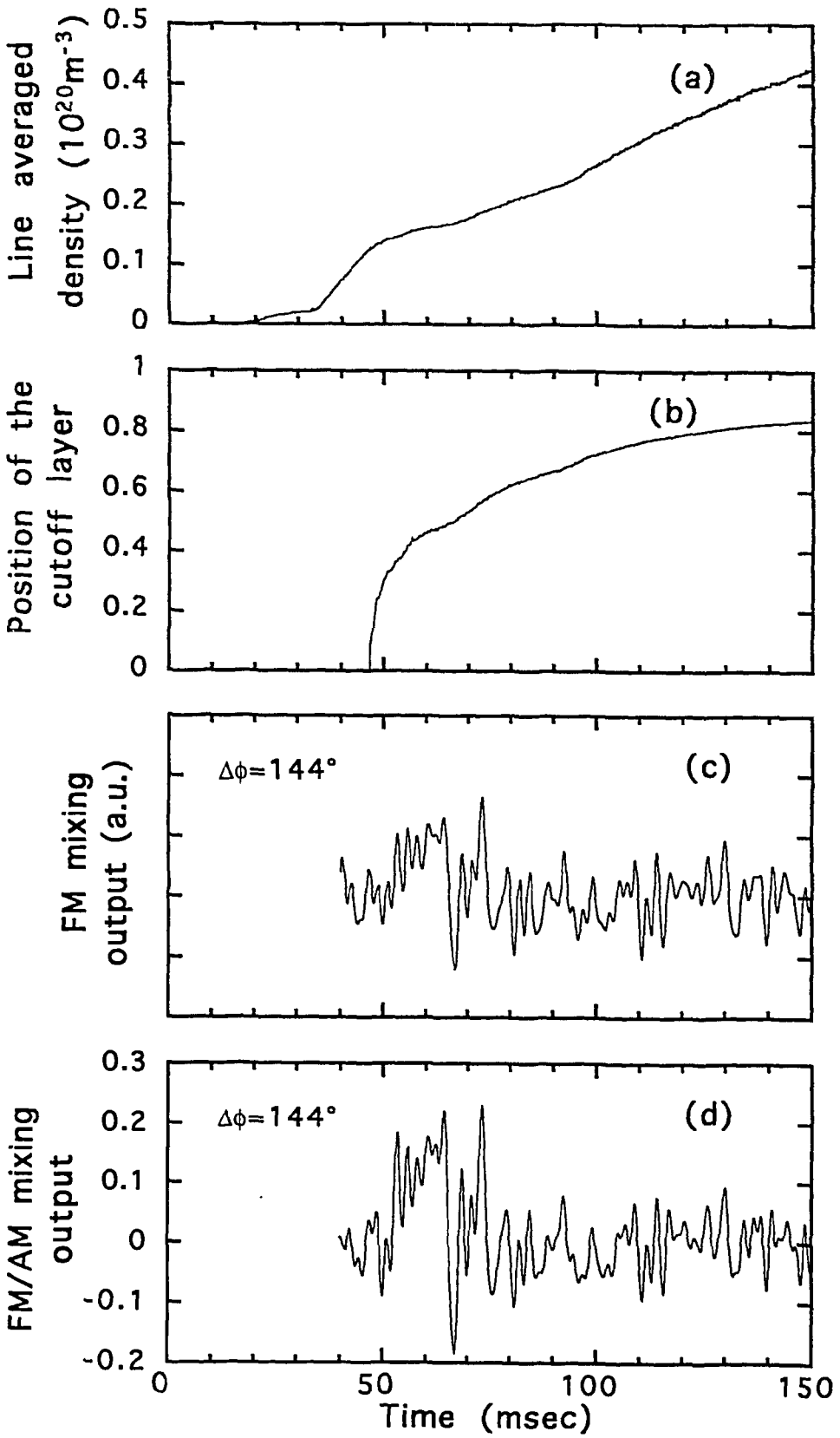
Line averaged density ($10^{20}m^{-3}$)
0.5
0.4
0.3
0.2
0.1
0
(a)
Position of the cutoff layer
1
0.8
0.6
0.4
0.2
0
(b)
FM mixing output (a.u.)
Δφ=144°
(c)
FM/AM mixing output
0.3
0.2
0.1
0
-0.1
-0.2
Δφ=144°
(d)
0
50
100
150
Time (msec)

Fig.7

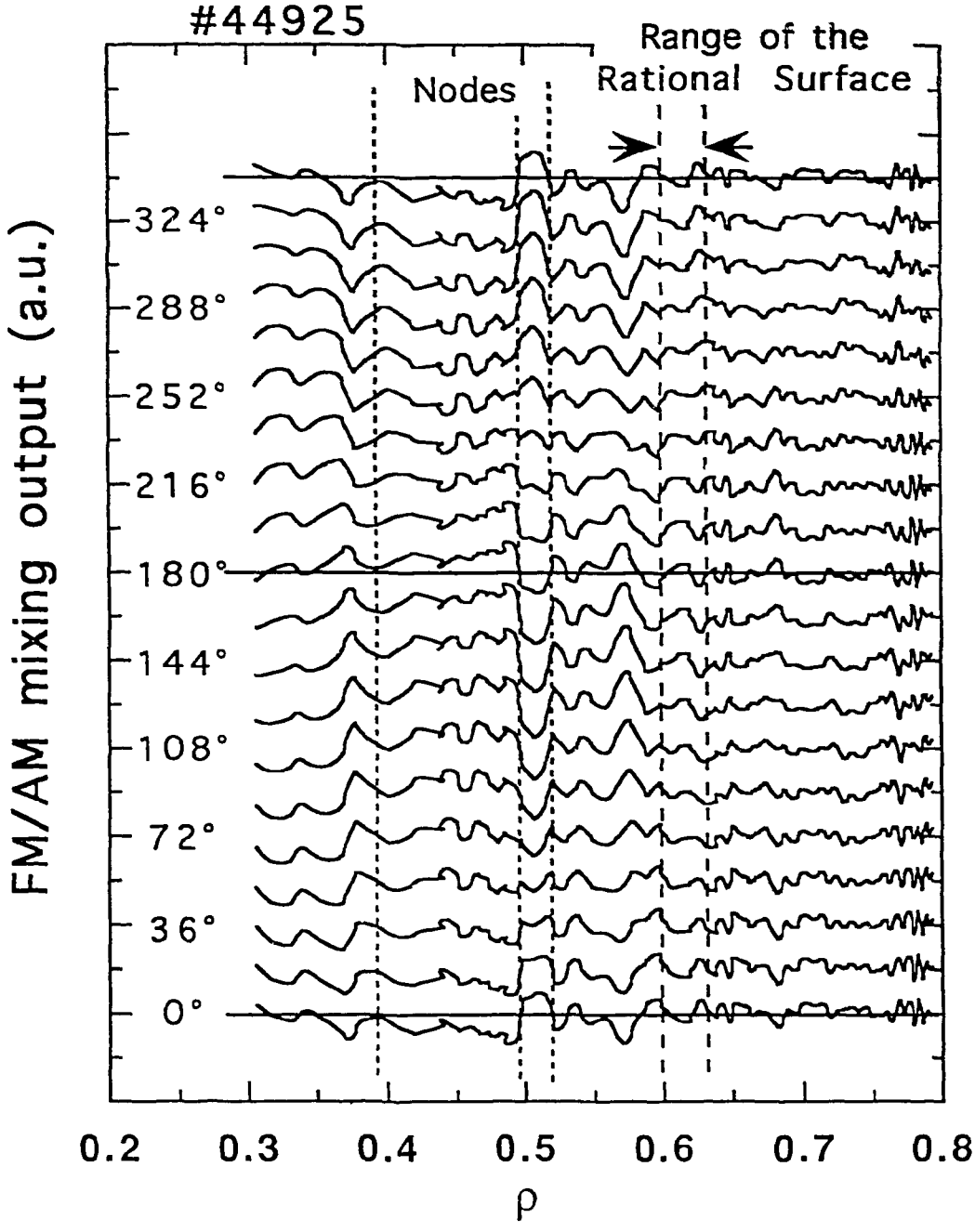
#44925
Range of the
Rational Surface
Nodes
324°
288°
252°
216°
180°
144°
108°
72°
36°
0°
FM/AM mixing output (a.u.)
0.2
0.3
0.4
0.5
0.6
0.7
0.8
ρ

Fig.8

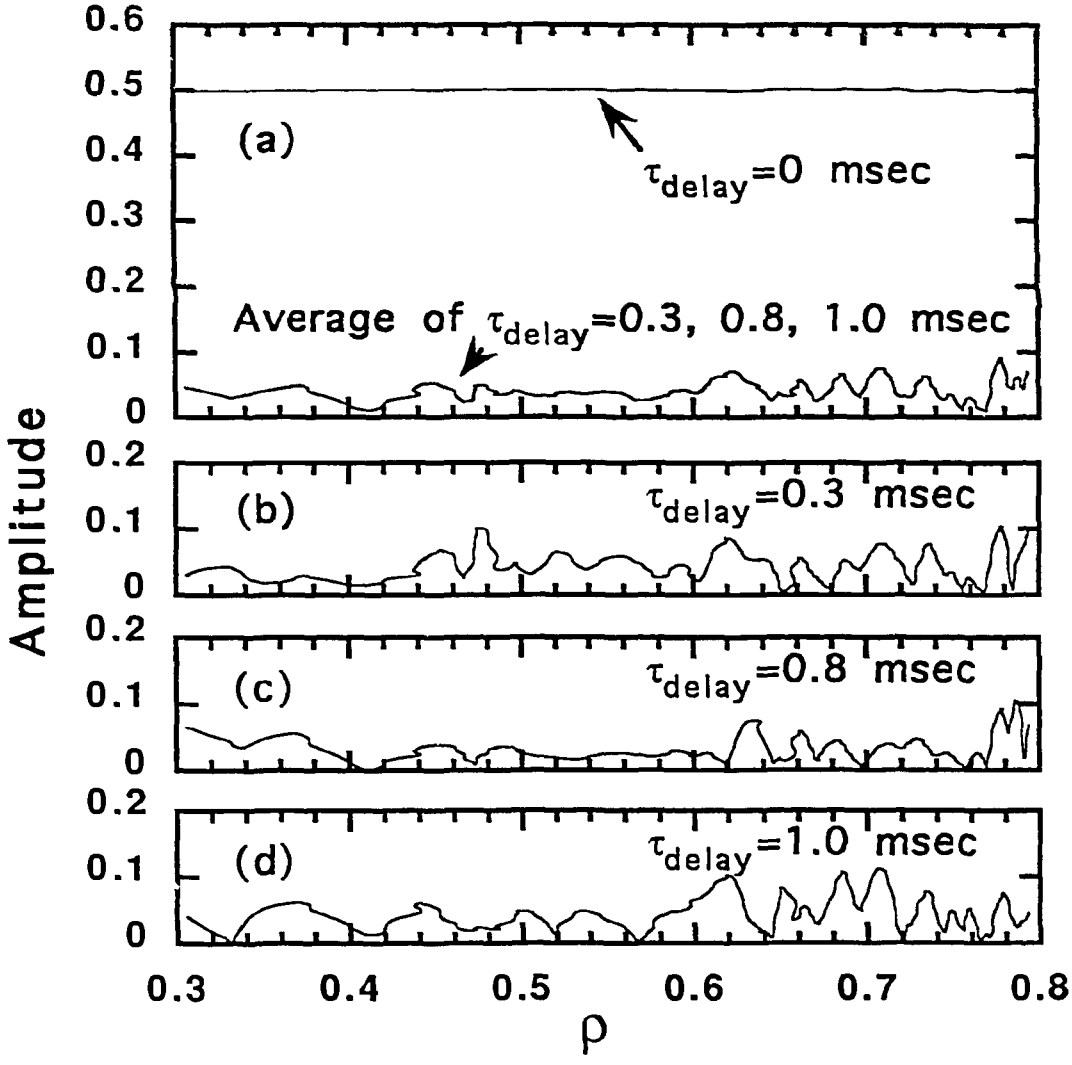
0.6
0.5
0.4
0.3
0.2
0.1
0
(a)
τ_{delay}=0 msec
Average of τ_{delay}=0.3, 0.8, 1.0 msec
0.2
0.1
0
(b)
τ_{delay}=0.3 msec
0.2
0.1
0
(c)
τ_{delay}=0.8 msec
0.2
0.1
0
(d)
τ_{delay}=1.0 msec
Amplitude
0.3
0.4
0.5
0.6
0.7
0.8
ρ

Fig.9

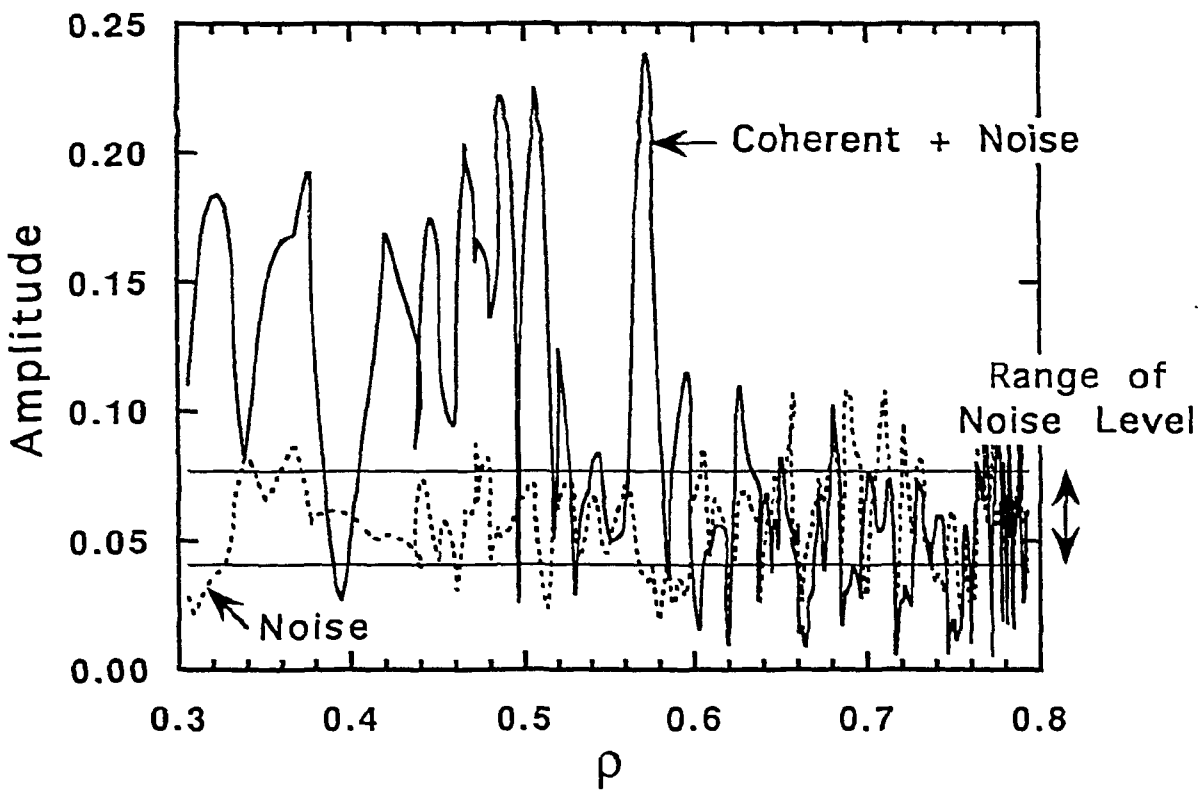
0.25
0.20
0.15
0.10
0.05
0.00
Amplitude
Coherent + Noise
Range of
Noise Level
Noise
0.3
0.4
0.5
0.6
0.7
0.8
ρ

Fig.10

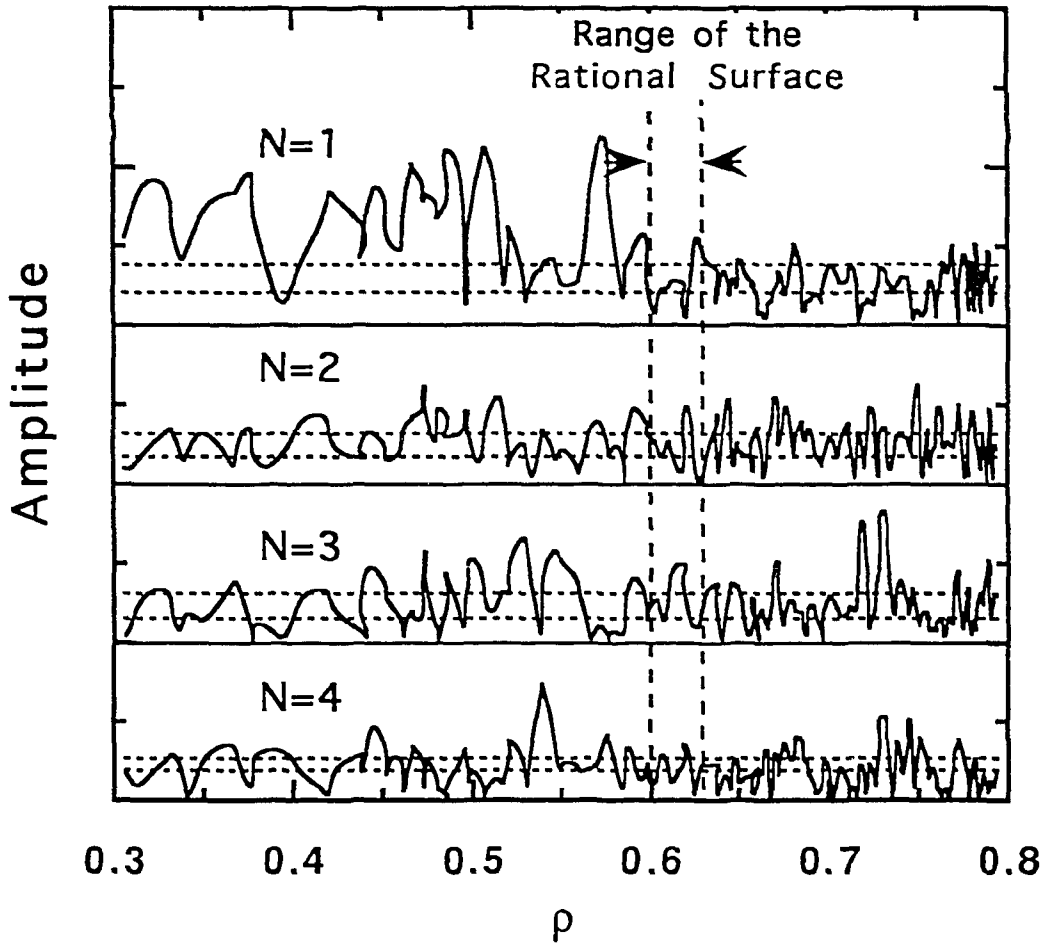
Range of the
Rational Surface
N=1
N=2
N=3
N=4
Amplitude
0.3
0.4
0.5
0.6
0.7
0.8
ρ

Fig.11

Recent Issues of NIFS Series

NIFS-300 H. Sugama and W. Horton,
Dynamical Model of Pressure-Gradient-Driven Turbulence and Shear Flow Generation in L-H Transition; Aug. 1994 (IAEA/CN-60/D-P-I-11)

NIFS-301 Y. Hamada, A. Nishizawa, Y. Kawasumi, K.N. Sato, H. Sakakita, R. Liang, K. Kawahata, A. Ejiri, K. Narihara, K. Sato, T. Seki, K. Toi, K. Itoh, H. Iguchi, A. Fujisawa, K. Adachi, S. Hidekuma, S. Hirokura, K. Ida, M. Kojima, J. Koog, R. Kumazawa, H. Kuramoto, T. Minami, I. Negi, S. Ohdachi, M. Sasao, T. Tsuzuki, J. Xu, I. Yamada, T. Watari,
Study of Turbulence and Plasma Potential in JIPP T-IIU Tokamak; Aug. 1994 (IAEA/CN-60/A-2-III-5)

NIFS-302 K. Nishimura, R. Kumazawa, T. Mutoh, T. Watari, T. Seki, A. Ando, S. Masuda, F. Shinpo, S. Murakami, S. Okamura, H. Yamada, K. Matsuoka, S. Morita, T. Ozaki, K. Ida, H. Iguchi, I. Yamada, A. Ejiri, H. Idei, S. Muto, K. Tanaka, J. Xu, R. Akiyama, H. Arimoto, M. Isobe, M. Iwase, O. Kaneko, S. Kubo, T. Kawamoto, A. Lazaros, T. Morisaki, S. Sakakibara, Y. Takita, C. Takahashi and K. Tsumori,
ICRF Heating in CHS; Sep. 1994 (IAEA-CN-60/A-6-I-4)

NIFS-303 S. Okamura, K. Matsuoka, K. Nishimura, K. Tsumori, R. Akiyama, S. Sakakibara, H. Yamada, S. Morita, T. Morisaki, N. Nakajima, K. Tanaka, J. Xu, K. Ida, H. Iguchi, A. Lazaros, T. Ozaki, H. Arimoto, A. Ejiri, M. Fujiwara, H. Idei, A. Iiyoshi, O, Kaneko, K. Kawahata, T. Kawamoto, S. Kubo, T. Kuroda, O. Motojima, V.D. Pustovitov, A. Sagara, C. Takahashi, K. Toi and I. Yamada,
High Beta Experiments in CHS; Sep. 1994 (IAEA-CN-60/A-2-IV-3)

NIFS-304 K. Ida, H. Idei, H. Sanuki, K. Itoh, J. Xu, S. Hidekuma, K. Kondo, A. Sahara, H. Zushi, S.-I. Itoh, A. Fukuyama, K. Adati, R. Akiyama, S. Bessho, A. Ejiri, A. Fujisawa, M. Fujiwara, Y. Hamada, S. Hirokura, H. Iguchi, O. Kaneko, K. Kawahata, Y. Kawasumi, M. Kojima, S. Kubo, H. Kuramoto, A. Lazaros, R. Liang, K. Matsuoka, T. Minami, T. Mizuuchi, T. Morisaki, S. Morita, K. Nagasaki, K. Narihara, K. Nishimura, A. Nishizawa, T. Obiki, H. Okada, S. Okamura, T. Ozaki, S. Sakakibara, H. Sakakita, A. Sagara, F. Sano, M. Sasao, K. Sato, K.N. Sato, T. Saeki, S. Sudo, C. Takahashi, K. Tanaka, K. Tsumori, H.Yamada, I. Yamada, Y. Takita, T. Tuzuki, K. Toi and T. Watari,
Control of Radial Electric Field in Torus Plasma; Sep. 1994 (IAEA-CN-60/A-2-IV-2)

NIFS-305 T. Hayashi, T. Sato, N. Nakajima, K. Ichiguchi, P. Merkel, J. Nührenberg, U. Schwenn, H. Gardner, A. Bhattacharjee and C.C.Hegna,
Behavior of Magnetic Islands in 3D MHD Equilibria of Helical Devices; Sep. 1994 (IAEA-CN-60/D-2-II-4)

NIFS-306 S. Murakami, M. Okamoto, N. Nakajima, K.Y. Watanabe, T. Watari, T. Mutoh, R. Kumazawa and T. Seki,
Monte Carlo Simulation for ICRF Heating in Heliotron/Torsatrons; Sep. 1994 (IAEA-CN-60/D-P-I-14)

NIFS-307 Y. Takeiri, A. Ando, O. Kaneko, Y. Oka, K. Tsumori, R. Akiyama, E. Asano, T. Kawamoto, T. Kuroda, M. Tanaka and H. Kawakami,
Development of an Intense Negative Hydrogen Ion Source with a Wide-Range of External Magnetic Filter Field; Sep. 1994

NIFS-308 T. Hayashi, T. Sato, H.J. Gardner and J.D. Meiss,
Evolution of Magnetic Islands in a Heliac; Sep. 1994

NIFS-309 H. Amo, T. Sato and A. Kageyama,
Intermittent Energy Bursts and Recurrent Topological Change of a Twisting Magnetic Flux Tube; Sep.1994

NIFS-310 T. Yamagishi and H. Sanuki,
Effect of Anomalous Plasma Transport on Radial Electric Field in Torsatron/Heliotron; Sep. 1994

NIFS-311 K. Watanabe, T. Sato and Y. Nakayama,
Current-profile Flattening and Hot Core Shift due to the Nonlinear Development of Resistive Kink Mode; Oct. 1994

NIFS-312 M. Salimullah, B. Dasgupta, K. Watanabe and T. Sato,
Modification and Damping of Alfvén Waves in a Magnetized Dusty Plasma; Oct. 1994

NIFS-313 K. Ida, Y. Miura, S -I. Itoh, J.V. Hofmann, A. Fukuyama, S. Hidekuma, H. Sanuki, H. Idei, H. Yamada, H. Iguchi, K. Itoh,
Physical Mechanism Determining the Radial Electric Field and its Radial Structure in a Toroidal Plasma; Oct. 1994

NIFS-314 Shao-ping Zhu, R. Horiuchi, T. Sato and The Complexity Simulation Group,
Non-Taylor Magnetohydrodynamic Self-Organization; Oct. 1994

NIFS-315 M. Tanaka,
Collisionless Magnetic Reconnection Associated with Coalescence of Flux Bundles; Nov. 1994

NIFS-316 M. Tanaka,
Macro-EM Particle Simulation Method and A Study of Collisionless Magnetic Reconnection; Nov. 1994

NIFS-317 A. Fujisawa, H. Iguchi, M. Sasao and Y. Hamada,
Second Order Focusing Property of 210° Cylindrical Energy Analyzer; Nov. 1994

NIFS-318 T. Sato and Complexity Simulation Group,
Complexity in Plasma - A Grand View of Self- Organization; Nov. 1994

NIFS-319 Y. Todo, T. Sato, K. Watanabe, T.H. Watanabe and R. Horiuchi,
MHD-Vlasov Simulation of the Toroidal Alfvén Eigenmode; Nov. 1994

NIFS-320 A. Kageyama, T. Sato and The Complexity Simulation Group,
Computer Simulation of a Magnetohydrodynamic Dynamo II; Nov. 1994

NIFS-321 A. Bhattacharjee, T. Hayashi, C.C.Hegna, N. Nakajima and T. Sato,
Theory of Pressure-induced Islands and Self-healing in Three-dimensional Toroidal Magnetohydrodynamic Equilibria; Nov. 1994

NIFS-322 A. Iiyoshi, K. Yamazaki and the LHD Group,
Recent Studies of the Large Helical Device; Nov. 1994

NIFS-323 A. Iiyoshi and K. Yamazaki,
The Next Large Helical Devices; Nov. 1994

NIFS-324 V.D. Pustovitov
Quasisymmetry Equations for Conventional Stellarators; Nov. 1994

NIFS-325 A. Taniike, M. Sasao, Y. Hamada, J. Fujita, M. Wada,
The Energy Broadening Resulting from Electron Stripping Process of a Low Energy Au^- Beam; Dec. 1994

NIFS-326 I. Vinlar and S. Sudo,
New Pellet Production and Acceleration Technologies for High Speed Pellet Injection System "HIPEL" in Large Helical Device; Dec. 1994

NIFS-327 Y. Hamada, A. Nishizawa, Y. Kawasumi, K. Kawahata, K. Itoh, A. Ejiri, K. Toi, K. Narihara, K. Sato, T. Seki, H. Iguchi, A. Fujisawa, K. Adachi, S. Hidekuma, S. Hirokura, K. Ida, M. Kojima, J. Koong, R. Kumazawa, H. Kuramoto, R. Liang, T. Minami, H. Sakakita, M. Sasao, K.N. Sato, T. Tsuzuki, J. Xu, I. Yamada, T. Watari,
Fast Potential Change in Sawteeth in JIPP T-IIU Tokamak Plasmas; Dec. 1994

NIFS-328 V.D. Pustovitov,
Effect of Satellite Helical Harmonics on the Stellarator Configuration; Dec. 1994

NIFS-329 K. Itoh, S-I. Itoh and A. Fukuyama,
A Model of Sawtooth Based on the Transport Catastrophe; Dec. 1994

NIFS-330 K. Nagasaki, A. Ejiri,
Launching Conditions for Electron Cyclotron Heating in a Sheared Magnetic Field; Jan. 1995

NIFS-331 T.H. Watanabe, Y. Todo, R. Horiuchi, K. Watanabe, T. Sato,
An Advanced Electrostatic Particle Simulation Algorithm for Implicit Time Integration; Jan. 1995

NIFS-332 N. Bekki and T. Karakisawa,
Bifurcations from Periodic Solution in a Simplified Model of Two-dimensional Magnetoconvection; Jan. 1995

NIFS-333 K. Itoh, S.-I. Itoh, M. Yagi, A. Fukuyama,
Theory of Anomalous Transport in Reverse Field Pinch; Jan. 1995

NIFS-334 K. Nagasaki, A. Isayama and A. Ejiri
Application of Grating Polarizer to 106.4GHz ECH System on Heliotron-E; Jan. 1995

NIFS-335 H. Takamaru, T. Sato, R. Horiuchi, K. Watanabe and Complexity Simulation Group,
A Self-Consistent Open Boundary Model for Particle Simulation in Plasmas; Feb. 1995

NIFS-336 B.B. Kadomtsev,
Quantum Telegragh : is it possible?; Feb. 1995

NIFS-337 B.B.Kadomtsev,
Ball Lightning as Self-Organization Phenomenon; Feb. 1995

NIFS-338 Y. Takeiri, A. Ando, O. Kaneko, Y. Oka, K. Tsumori, R. Akiyama, E. Asano, T. Kawamoto, M. Tanaka and T. Kuroda,
High-Energy Acceleration of an Intense Negative Ion Beam; Feb. 1995

NIFS-339 K. Toi, T. Morisaki, S. Sakakibara, S. Ohdachi, T.Minami, S. Morita, H. Yamada, K. Tanaka, K. Ida, S. Okamura, A. Ejiri, H. Iguchi, K. Nishimura, K. Matsuoka, A. Ando, J. Xu, I. Yamada, K. Narihara, R. Akiyama, H. Idei, S. Kubo, T. Ozaki, C. Takahashi, K. Tsumori,
H-Mode Study in CHS; Feb. 1995

NIFS-340 T. Okada and H. Tazawa,
Filamentation Instability in a Light Ion Beam-plasma System with External Magnetic Field; Feb. 1995

NIFS-341 T. Watanbe, G. Gnudi,
A New Algorithm for Differential-Algebraic Equations Based on HIDM; Feb. 13, 1995

NIFS-342 Y. Nejoh,
New Stationary Solutions of the Nonlinear Drift Wave Equation; Feb. 1995